et al. (2011) have demonstrated that the slag content increases in proportion to its apparent chargeability. A detailed analysis shows that the sixteenth-century mine produced ~ 7.6 tons of slag, corresponding to ~ 6.9 tons of commercial iron.

5.7 Self-potential (SP): introduction

Under natural conditions, without any introduction of an artifical current into the ground as in the resistivity/IP methods, various modes of electric charge imbalance or accumulation are found to spontaneously develop in the subsurface (Jouniaux *et al*., 2009). The resulting self-potentials, which can be measured using pairs of electrodes deployed at the surface or less commonly in boreholes, are very stable in time and are generally in the range of ± 100 mV or higher. A voltmeter is used to measure the SP signals; it should have a high sensitivity (0.1 mV) and a high input impedance (typically >100 MΩ) compared to that of the ground between the two electrodes.

In near-surface applications, commonly, one of the electrodes is held at a fixed location and used as a base or reference station while the other electrode is moved from place to place across an area under investigation. The potential difference between the roving electrode and the reference electrode is the quantity that is measured. In more sophisticated setups, a multi-electrode array of electrodes can also be deployed for monitoring the spatiotemporal changes in SP signals across the survey area. In such cases, the potentials at the various electrodes comprising the array, relative to the potential of the fixed electrode, are recorded periodically by a multiplexed voltmeter.

Self-potential data should always be corrected prior to interpretation for temporal drift and topographic effects (Zhou *et al*., 1999). A topographic correction is required since SP signals tend to increase in the downhill direction, along the local hydraulic gradient. It has also been commonly observed that SP readings are noisier in heavily vegetated areas, relative to sparsely vegetated areas, due to bioelectric activity. To ensure good electrical contact with the ground, electrodes can be inserted into shallow augured holes filled with a mud slurry.

Example. SP mapping of the groundwater system at Stromboli volcano.

An SP survey conducted on the persistently active Stromboli volcano in the Tyrrhenian Sea, Italy, is reported by Finizola *et al*. (2006) with the goal to identify subsurface groundwater flow patterns. Detection of aquifers on volcanic islands is required for improved water-resource management and also better hazard assessment since water can react violently with magma and cause dangerous phreatic eruptions. The SP data with 20-m station spacing are shown in Figure 5.9 along with a co-located 2-D inversion of resistivity data using the Wenner electrode configuration (see Chapter 4). The hydrothermal system beneath Stromboli summit is easily recognized by the strong SP variations within the region of lowest resistivity, i.e. the rightmost shaded region marked C on the figure.

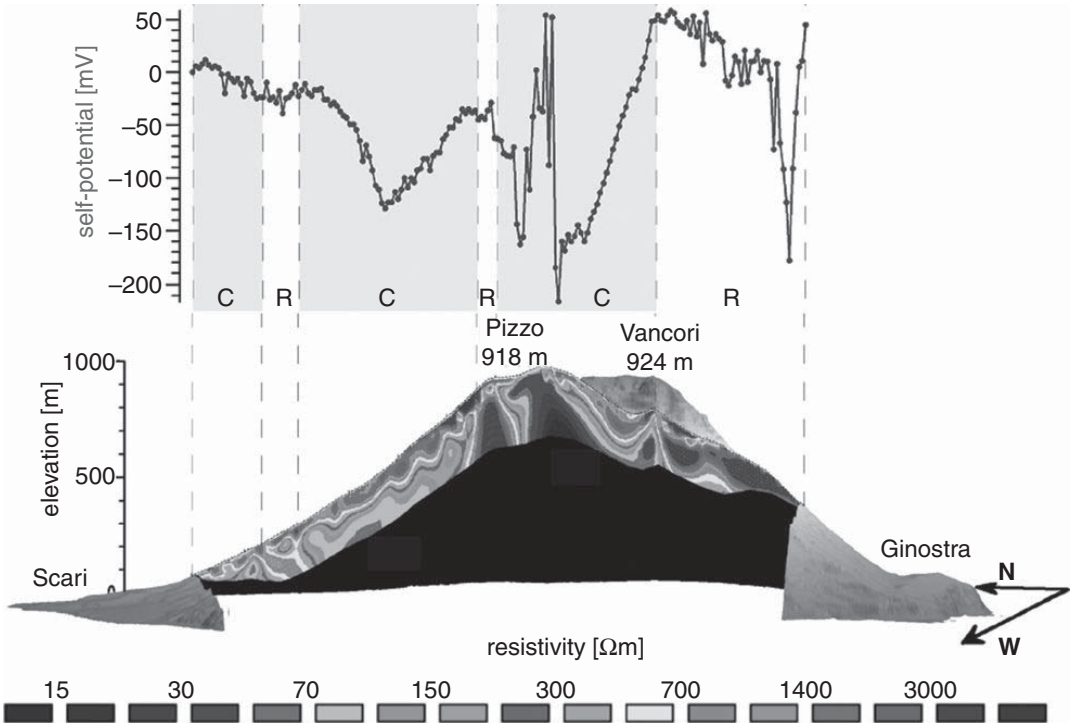

Figure 5.9 SP signals and 2-D electrical resistivity structure at Stromboli volcano, Italy. C = conductive zone; R = resistive zone. After Finizola *et al*. (2006).

5.8 Physical mechanisms

Subsurface charge accumulations may be sustained by a number of physical and electrochemical processes. Large SP anomalies, up to hundreds of mV, for example, have long been measured in association with zones of metal sulfide and oxide mineralization. An enduring theory purporting to explain the so-called *mineralization potential* of sulfide bodies is due to Sato and Mooney (1960). Stable SP anomalies of comparable magnitude may also be registered in the presence of metallic cultural noise such as pipelines, steel well casings, metallic fences, and utility boxes (Revil *et al*., 2012). This type of SP signal is caused by the movement of electrons in response to spatial variations in the redox potential at heterogeneous metal–electrolyte interfaces.

Another common mechanism that generates a spontaneous potential involves the movement of electrolytic groundwater through a porous rock. A *streaming potential*, for example, develops when pore-fluid electrolyte flows in response to a pressure and/or thermal gradient. Due to the presence of the electric double layer at the mineral surface (Figure 5.6), the fluid flow carries an excess of the mobile counter ions resident in the bulk electrolyte, relative to a deficit of ions of the opposite sign that constitute the immobile fixed layer. This differential movement of ions and counter ions is equivalent to an electric

current. An effective resistance to the current is provided by the electrolyte viscosity η, its resistivity ρ, and the *zeta potential* ζ (the potential difference between the charged mineral surface and an arbitrary point within the neutral bulk electrolyte). The streaming potential is nothing more than the resulting electrical potential drop between two points along the path of the fluid flow (e.g. Rice and Whitehead, 1965; Levine *et al*., 1975). A streaming potential of this type often arises as pore electrolytes flow in response to an external mechanical disurbance; this constitutes the fundamental basis for the *seismoelectric effect* to be discussed in Chapter 10.

A different type of SP effect occurs at the liquid–liquid interface between two pore fluids that are characterized by different concentrations of ions in solution. There will be a net transfer of ions across the junction as the more-concentrated solution diffuses into the less-concentrated solution. Since cations and anions generally have different mobilities, the rates of diffusion of the different charged species across the interface are unequal. The differential movement of ions leads to the development of a net charge distribution on the liquid–liquid interface, thereby generating a liquid junction or *diffusion potential*. A sharp contrast in solution concentration is not required, as a diffusion potential can also occur in the presence of a salinity gradient.

It has long been recognized in geophysical well-logging that a spontaneous potential develops at junctions between permeable sand and less-permeable shale beds. Suppose the pore fluid is an ideal electrolyte consisting of NaCl only. Due to its layered clay structure and charged mineral surfaces, the shale is somewhat permeable to the Na^+ cations but it is relatively impervious to the Cl^- anions. Suppose the shale bed separates two sand beds which contain different NaCl concentrations. There will be a net migration of Na^+ cations across the shale bed from the more-concentrated toward the less-concentrated solution. Since shales preferentially pass the cations and restrict the anions, they act much like an ion-selective membrane (Bard and Faulkner, 1980). The differential movement of ions in shale beds generates the *membrane potential* that is measured by a downhole voltmeter.

The *thermoelectric effect* can also be a significant source of SP signals in geothermal systems, volcanoes, near-underground coal fires, and in other geological settings that are characterized by persistent spatial variations in subsurface temperature. The thermoelectric effect is the appearance of a voltage across a sample of geomaterial that is not of a uniform temperature. A temperature gradient causes mobile charge carriers within the geomaterial to migrate from regions of elevated temperature to regions of cooler temperature. The differential movement of charge carriers of different species establishes a non-uniform subsurface charge distribution. The thermoelectric coupling coefficient [mV/°C] is defined as the ratio $\Delta V/\Delta T$ of the voltage to temperature difference. Zlotnicki and Nishida (2003) report values of the order of ~ 0.1–1.0 mV/°C.

Finally, Minsley *et al*. (2007) have shown that subsurface spatial variations in electrical conductivity can also have an effect on potential measurements made at the surface. However, it is often difficult to estimate the magnitude of this effect in practical situations since the underground distribution of electrical conductivity is rarely known.

5.9 Interpretation of SP measurements

Since SP signals are generated by equal and opposite charge distributions, as indicated schematically in Figure 5.1, an SP source may be modeled as an assemblage of electric dipoles. Recall that an electric dipole is the simplest possible distribution of equal and opposite charge, namely a positive point charge q and a negative point charge $-q$ separated by a distance d. The electric dipole moment is given by $m = qd$. A polarized sphere, in which the positive charge is distributed over one hemisphere and the negative charge is distributed over the other hemisphere, may be represented at large distances relative to its radius by an equivalent electric dipole of moment M.

Polarized sphere. It is straightforward to calculate the electric potential due to a polarized sphere. As shown in Figure 5.10a, suppose the sphere is polarized in the vertical plane $y = 0$ in a direction that makes angle α with respect to the x-axis so that

$$\mathbf{M} = M\cos\alpha\,\hat{\mathbf{x}} + M\sin\alpha\,\hat{\mathbf{z}}. \tag{5.10}$$

The electric potential V of an equivalent electric dipole of moment $\mathbf{M}$ is given by the standard formula (e.g. Blakely, 1995)

$$V = -\frac{\mathbf{M}\cdot\nabla}{4\pi\varepsilon_0}\frac{1}{R} \tag{5.11}$$

where $\varepsilon_0 = 8.85 \times 10^{-12}$ F/m is the permittivity of free space and

$$R = |\mathbf{r}_P - \mathbf{r}_Q| = \sqrt{(x - x_0)^2 + z_0^2} \tag{5.12}$$

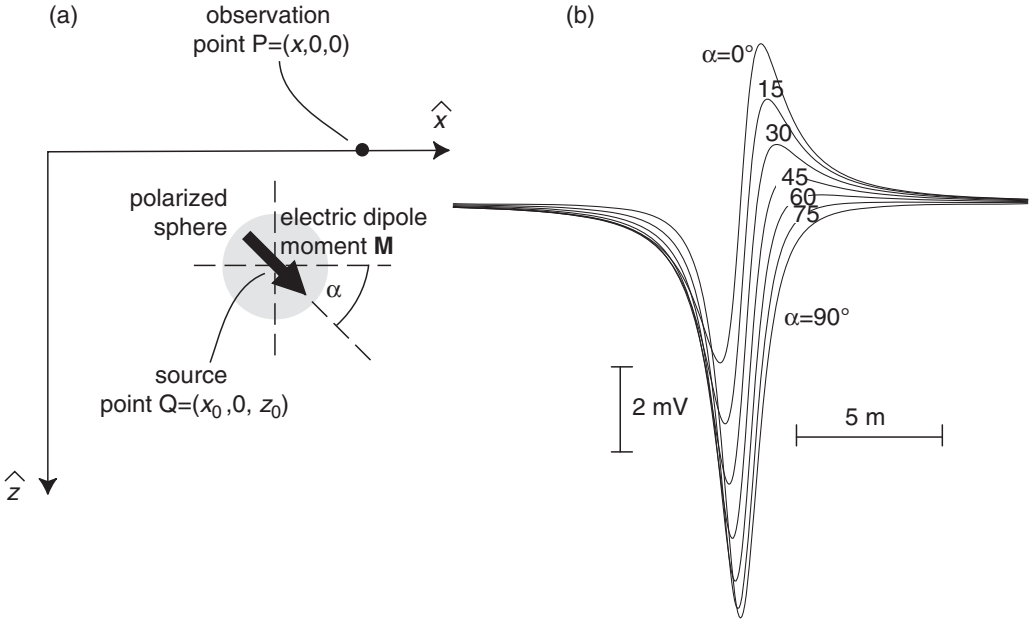

Figure 5.10 (a) A polarized sphere modeled as an electric dipole. (b) The SP response of a buried polarized sphere for different angles of polarization.

is the distance between the dipole at source location $Q = (x_0, 0, z_0)$ and the observation point at Earth's surface, $P = (x, 0, 0)$. Inserting Equations (5.10) and (5.12) into Equation (5.11) results in

$$V(x) = \frac{M}{4\pi\varepsilon_0} \frac{(x - x_0)\cos\alpha - z_0 \sin\alpha}{[(x - x_0)^2 + z_0^2]^{3/2}}. \tag{5.13}$$

The function $V(x)$ is plotted in Figure 5.10b for different values of the angle of polarization from $= 0^\circ$, aligned with the $+x$-axis, to $\alpha = 90^\circ$, aligned with the $+z$-axis. The sphere is buried at depth $z_0 = 1.0$ m and located at $x_0 = 0$. The dipole moment is $M = 10^6$ Cm. Finding a similar analytic solution for the SP response of a long horizontal cylinder is left as an exercise for the reader.

Polarized dipping sheet. Another simple geological scenario for which the SP response is amenable to an analytic treatment is fluid flow within a dipping planar fault structure. The fault plane can be modeled as an electrically polarized thin sheet, or ribbon, of half-width a embedded in a host medium of uniform resistivity ρ (Paul, 1965), as shown in Figure 5.11a. One edge of the sheet is represented as a line of negative charges of density $-\Sigma$ [C/m] while the other is a line of positive charges of density $+\Sigma$ [C/m]; both lines extending from $-\infty$ to $+\infty$ in the along-strike ($\pm y$) direction.

The electric potential V due to a line of charges has the well-known logarithmic form (e.g. Blakely, 1995)

$$V_\pm = \pm\frac{\Sigma\rho}{\pi} \ln\left(\frac{1}{r_\pm}\right), \tag{5.14}$$

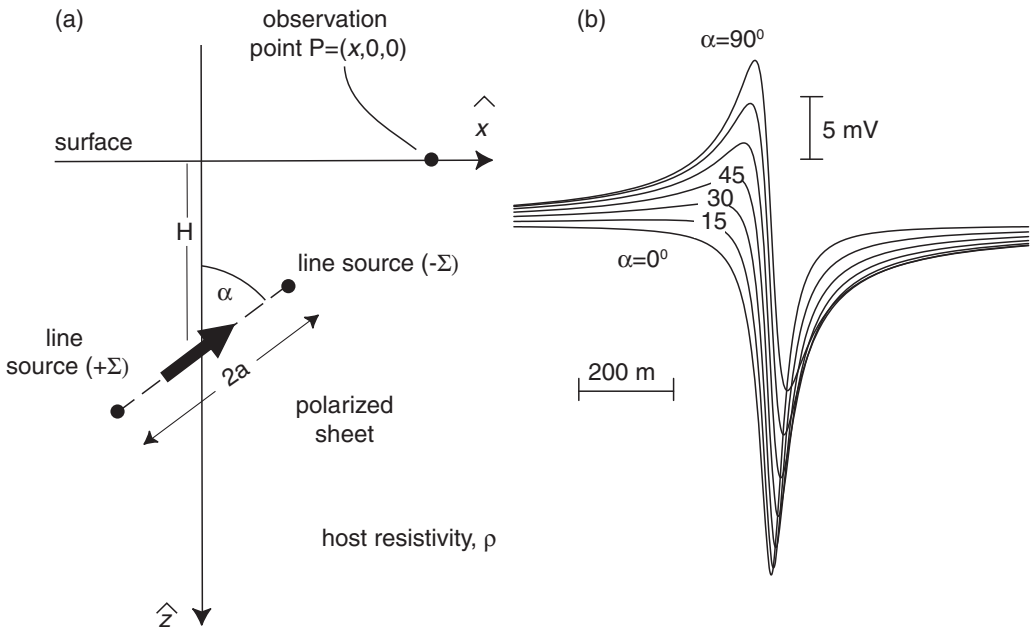

Figure 5.11 (a) A polarized, inclined sheet modeled as an electric line charges. (b) The SP response of a buried polarized sheet for different angles of inclination.

where $r_{\pm}$ is the distance from the observation point to the positive and negative line of charges, respectively. A glance at the geometry in the figure shows that

$$r_{-} = \sqrt{(x - a\cos\alpha)^2 + (H - a\sin\alpha)^2}; \tag{5.15}$$

$$r_{+} = \sqrt{(x + a\cos\alpha)^2 + (H + a\sin\alpha)^2}; \tag{5.16}$$

from which it readily follows

$$\ln\left(\frac{1}{r_{-}}\right) = -\frac{1}{2}\ln[(x - a\cos\alpha)^2 + (H - a\sin\alpha)^2]; \tag{5.17}$$

$$\ln\left(\frac{1}{r_{+}}\right) = -\frac{1}{2}\ln[(x + a\cos\alpha)^2 + (H + a\sin\alpha)^2]. \tag{5.18}$$

The total SP signal due to the two lines of charges is the sum of the potentials due to each sheet, namely, $V = V_{+} + V_{-}$. Adding the two contributions using the above equations results in

$$V = \frac{\Sigma\rho}{2\pi}\left\{\ln[(x - a\cos\alpha)^2 + (H - a\sin\alpha)^2] - \ln[(x + a\cos\alpha)^2 + (H + a\sin\alpha)^2]\right\}, \tag{5.19}$$

which is plotted at Figure 5.11b for different values of the angle α. The following parameters are used: $\Sigma = \pm 0.01$ C/m, $\rho = 10.0$ Ωm, fault-zone half-width $a = 10$ m, and depth of burial $H = 30$ m.

A number of rules can be inferred from the analytic solutions which relate the width of an SP anomaly to the depth of an idealized source. For example, it is easy to show that the depth to a point charge is given by $d = x_{0.5}/\sqrt{12}$, where $x_{0.5}$ is the FWHM of the corresponding SP anomaly, i.e. its width at one-half its maximum value. Similarly, the depth rule for a vertically polarized sphere is $d \sim 0.65x_{0.5}$.

Self-potential surveys often provide useful hydrological information about fractures and karst conduits since streaming-potential anomalies have long been associated with divergent groundwater flow (Lange and Barner, 1995). As illustrated schematically in Figure 5.12, residual SP anomalies, after drift and topographic corrections have been made, are generally positive over groundwater discharges at springs and negative over groundwater infiltration at sinkholes.

5.10 Continuous wavelet transform analysis

The continuous wavelet transform (CWT) was introduced in Chapter 2 as a means for analyzing non-stationary data series. In this section we will see that the CWT can also be used for interpreting potential field measurements in terms of the geometry of the causative source and its depth of burial. The underlying theory is developed in Moreau *et al*. (1997, 1999) and has since been applied to many types of geophysical data including magnetics by Vallee *et al*. (2004). Here we outline the application of CWT for analysis of SP data